AGU PUBLICATIONS

Geophysical Research Letters

RESEARCH LETTER
10.1002/2014GL062260

**Key Points:**
- New high-resolution climatology in the EAC separation zone from gliders
- Upwelling associated with EAC encroachment and separation is mapped
- Depth-averaged momentum balance reveals the determinant role of advection

**Correspondence to:**
A. Schaeffer,
a.schaeffer@unsw.edu.au

**Citation:**
Schaeffer, A., and M. Roughan (2015), Influence of a western boundary current on shelf dynamics and upwelling from repeat glider deployments, *Geophys. Res. Lett.*, *42*, 121–128, doi:10.1002/2014GL062260.

Received 17 OCT 2014
Accepted 8 DEC 2014
Accepted article online 11 DEC 2014
Published online 13 JAN 2015

# Influence of a western boundary current on shelf dynamics and upwelling from repeat glider deployments

**A. Schaeffer[1] and M. Roughan[1]**

[1]School of Mathematics and Statistics, University of New South Wales, Sydney, New South Wales, Australia

**Abstract** The separation zone of a dynamically important western boundary current (WBC) is resolved through a series of sustained glider deployments along the coastal edge of the jet. The comprehensive data set from 23 missions (2008–2014) provides a new high-resolution hydrographic climatology which is exploited to understand the spatial extent of dense water uplift and the depth-averaged momentum balances across the East Australian Current (EAC) separation zone. The predominantly geostrophic shelf circulation and temperature fields are least (most) variable upstream (downstream), where encroachment (separation) dominates. For the first time we resolve the nonlinear advection terms which are considerable in the along-shelf momentum balance. Near bottom water masses indicate dense water uplift, as a result of the EAC encroachment and separation. The data provide both new insight into and a climatology of separation-induced uplift and demonstrate a successful model for repeat glider missions in a dynamic WBC environment.

## 1. Introduction

The separation zone of a western boundary current (WBC) is a dynamically important region, characterized by highly variable circulation along the coast. Upwelling is also favored by the separation of the jet, influencing the water mass properties and in turn the biological productivity. However, the inherent strong currents (2 m $s^{-1}$) and dynamic nature of the separation zone increases the challenge of sustainably observing the subsurface properties. Here we show the first in situ observations that resolve the spatial (subsurface) extent of uplift and upwelling on the shelf associated with the separation of the WBC jet from the eastern Australian coast. Previous observational studies in the region have shown that geostrophy is the main balance across the shelf adjacent to the East Australian Current (EAC) [*Oke et al.*, 2003; *Schaeffer et al.*, 2013, 2014a]; however, data limitations have precluded the estimation of the advection terms, shown to be important in the modeling studies of *Oke and Middleton* [2000]; *Roughan et al.* [2003]. Here we describe the spatial structure of water masses and make estimates of the momentum balances in the separation zone of the East Australian Current (EAC) using 6 years of sustained glider measurements which made 33,000 CTD (conductivity-temperature-depth) profiles between the coast and the 200 m isobath.

The EAC is the poleward flowing WBC of the South Pacific Ocean. It has been well documented in terms of transport [*Mata et al.*, 2000; *Ridgway et al.*, 2008], intrusions onto the shelf [*Schaeffer et al.*, 2013, 2014b], and long-term trends [*Oliver and Holbrook*, 2014]. The region where the EAC separates from the coast (30.7°S–32.4°S, 50% of the time) [*Cetina-Heredia et al.*, 2014] is very energetic, while downstream, eddies are shed [*Mata et al.*, 2006; *Suthers et al.*, 2011] and poleward transport is primarily eddy driven [*Cetina-Heredia et al.*, 2014]. Moored observations from upstream and downstream of the EAC separation [*Schaeffer et al.*, 2013, 2014a; *Wood et al.*, 2013] and from a 3 month deployment straddling the separation zone [*Roughan and Middleton*, 2004] indicate the presence of a strong poleward stratified current upstream and weaker variable currents downstream. However, this is the first observational study to characterize the signature of the EAC through the water column across the EAC separation zone in a quasi-synoptic manner with sufficiently high cross-shelf resolution.

The EAC has also been shown to drive dense water uplift (bottom Ekman transport) in response to intense bottom stress at both 30°S and 34°S (from mooring arrays [*Schaeffer et al.*, 2014b]). Through an idealized modeling study, *Oke and Middleton* [2001] suggested that outcropping of the dense water is favored at the separation zone where the current deviates eastward from the coast. This "separation induced upwelling" has also been observed from shipboard hydrographic observations around 32°S [*Roughan and Middleton*, 2002], while satellite observations have been used to infer the frequency of both wind and

current upwelling [*Rossi et al.*, 2014] and its biological implications [*Everett et al.*, 2014]. Despite the efforts above, estimates of the subsurface spatial structure of dense water uplift were limited regionally [*Armbrecht et al.*, 2014a, 2014b] or to modeling studies due to data limitations.

A thorough understanding of the local mechanisms driving both the along-shelf and across-shelf dynamics is also lacking. In particular, the role of advection is yet to be quantified from observations. In the along-shelf momentum equation, *Oke et al.* [2003] found that the root mean square (RMS) of the across-shore advection term was greater than the stress terms. The dominant terms during the advection of a thermal front were the local acceleration and the residual (which included the pressure gradient, along-shelf advection, and calculation errors), suggesting strongly nonlinear dynamics. Other attempts to resolve alongshore advection terms have been confined to modeling studies. *Roughan et al.* [2003] showed the significance of advection in the along-shelf balance with a change in sign of the advective terms in the EAC separation region evident in a climatological modeling study. The implications of horizontal advection were shown by *Oke and Middleton* [2000] when investigating the influence of advective acceleration on the bottom boundary layer (BBL) dynamics. They found a link between horizontal advection and vertical diffusion, interfering with the geostrophic adjustment of the BBL and thus providing a sustained mechanism for upwelling.

We present new insights into both the shelf hydrography and dynamics gained from glider observations, including the first water mass and a momentum balance analysis spanning the EAC separation zone. We are able to resolve the alongshore advection terms which to date have been impossible to measure with traditional techniques in this dynamic separation region. These results are obtained from the high-resolution climatological data set generated from multiple ocean glider deployments (described in section 2). Section 3 presents the results, focusing on the EAC signature on the shelf and the corresponding dynamical balances which are then discussed in the context of previous studies (section 4).

## 2. Data and Methods

### 2.1. Deployment Strategy

A total of 23 ocean gliders were deployed off southeastern Australia from 2008 to 2014. While the early deployments were more eddy-oriented [e.g., *Baird et al.*, 2011] a sustainable deployment strategy has since been adopted (12 deployments from 2010 to mid-2014) using shallow Slocum gliders that dive to a maximum depth of 200 m. The strategy consists of three to four deployments per year, spanning different seasons, with a consistent start location and navigation plan. The gliders are deployed off Yamba (29.5°S) in ~40 m of water and are directed offshore to the 200 m isobath before returning to the coast. In this way they zigzag poleward along the continental shelf bounded by the 200 m isobath (Figure 1a). Typically, recovery (which is determined by battery usage and oceanographic conditions) occurs after around 3 weeks and an average of 3000 dives, spanning the EAC separation zone from 30 to 32.5°S. This deployment strategy results in quasi-synoptic observations of the continental shelf waters with high spatial coverage, which are not aliased by seasonal variability within missions.

### 2.2. Parameters Measured

Data from two types of gliders (Seagliders and Slocums) have been used, which are usually instrumented with a pumped Seabird CTD (conductivity-temperature-depth; sampling frequency 0.2–0.8 Hz), a WETLabs BBFL2SLO, and an Aanderaa Oxygen optode [*Baird et al.*, 2011; *Schaeffer et al.*, 2014b]. Horizontal depth-averaged velocity during the dead-reckoning navigation is obtained from the GPS location differences at each surfacing. Uncertainties can arise from, for example, uncertainties in the pitch and heading [*Merckelbach et al.*, 2008]. However, velocities in this region are generally 1 to 2 orders of magnitude greater than these estimated errors. The data set quality control was conducted following Argo standards, including a salinity spike correction [*Wong et al.*, 2014]. Only physical parameters (temperature, salinity, density, and velocity) are investigated in this study.

### 2.3. Shelf Climatology

To amalgamate all the observations, we create a spatial grid in the domain, binning the continental shelf between 29 and 34°S at intervals of 0.25° in latitude. Across the shelf, due to the varying shelf width, we consider bins based on the water depth. Intervals are 20–50 m, 50–80 m, 80–110 m, 110–140 m, and 140–200 m. While this leads to a coarser along-shelf spatial resolution, *Oke and Sakov* [2012] showed that sea surface height, sea surface temperature, and near-surface velocities are correlated over long distances along the southeastern Australian shelf. In particular, complex near-surface velocity correlations appear to

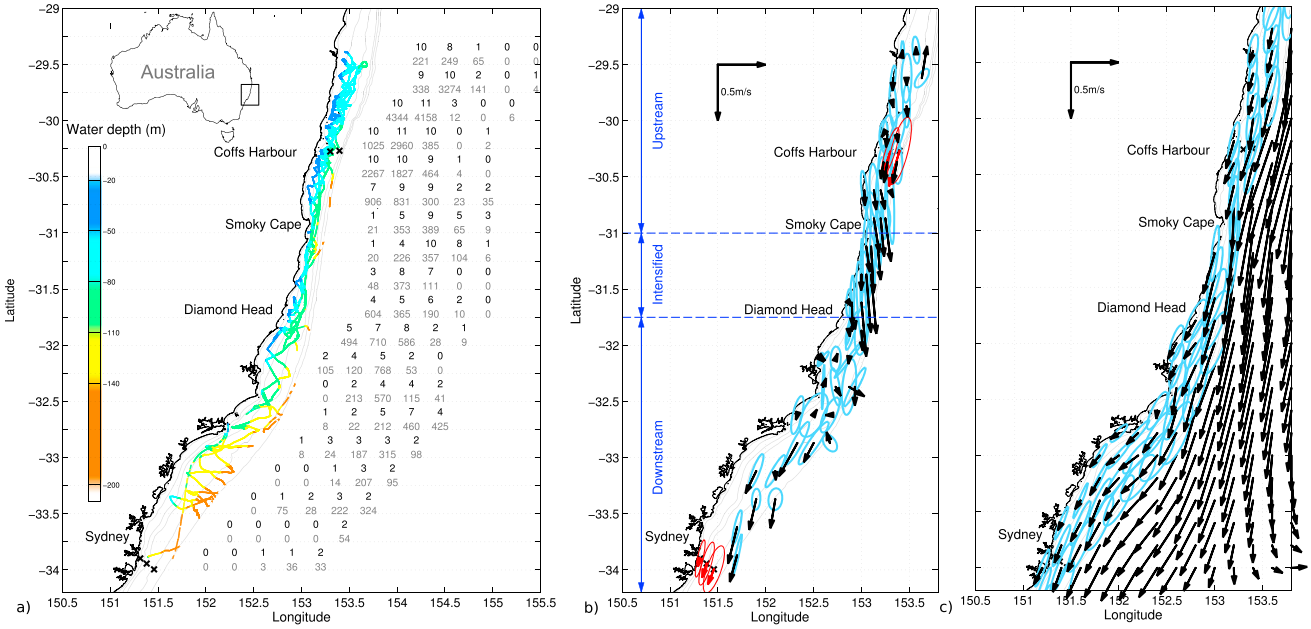


**Figure 1.** (a) Location of the study area and glider tracks for the 23 glider deployments over the southeastern Australian shelf. Along-track colors indicate bottom depth intervals (m) used for the cross-shelf discretization (20–50 m, 50–80 m, 80–110 m, 110–140 m, and 140–200 m). For each latitude, the number of glider missions (bold) and total dives >25 m are indicated for the five cross-shelf bins. (b) Binned mean current vectors and variance ellipses from glider depth-averaged velocities (in black and light blue) and from moored current-meter measurements (in red) off Coffs Harbour (CH070 and CH100) and Sydney (ORS065, SYD100, and SYD140) between 2010 and 2013. (c) Mean current vectors and variance ellipses from altimetry-derived geostrophic velocities between 2009 and 2013. Contours of 20, 50, 80, 110, 140, and 200 m isobaths are shown.

be greater than 0.8 within 1° of latitude of the Australian Integrated Marine Observing System mooring locations (30°S and 34°S) in the along-shelf direction. Figure 1a shows each of the different glider tracks relative to this griding system. The number of gliders passing through each bin ranged between 0 and 11 gliders (Figure 1a). Bins with ≤1 glider passing through or ≤30 profiles are not included to minimize seasonal aliasing. High-frequency tidal variability, weak in the region [*Arbic et al.*, 2010], is filtered out when averaging measurements as the average time a glider spends in a bin is ~27 h.

The average number of dives per bin is ~560, reaching > 4300 at 30°S. On the shelf, an average dive takes 11 min, is 55 m deep with a vertical resolution of ~2 m, and travels a distance of ~200 m. Only upcasts are used as the CTD is considered to receive cleaner flow during ascent [`?Rudnick2011`]. Temperature and salinity were integrated and depth averaged over both the top and bottom 20 m within each spatial bin in order to compare the surface and bottom boundary layers. Depth-averaged currents were averaged within a bin. The cross-shelf and along-shelf binning results in a new high-resolution climatology of the shelf in situ hydrography and depth-averaged velocity. This gridded data set was also used to estimate terms of the depth-averaged momentum balances (section 3.3). Baroclinic pressure gradients between adjacent bins were computed from density measurements gridded at 1 m vertical resolution. Other terms were obtained from depth-integrated current gradients, by forward difference between the center of adjacent bins. Bins were separated by 28 km alongshore and between 3 km and 31 km across-shelf (average of 7 km). Estimates of the variance of each term (standard deviations) are used to illustrate their relative influence in the momentum balances.

## 3. Results

### 3.1. Structure of the Velocity Field

The spatial distribution of the binned glider-derived velocities (Figure 1b) shows a dominant southward flow. This is consistent with the influence of the EAC, as shown in the mean geostrophic current field (Figure 1c) constructed from both altimetry and coastal tide gauge observations around Australia [*Deng et al.*, 2010]. Importantly, the glider data set resolves more of the fine-scale circulation structure on the shelf. The maximum mean depth-averaged velocity appears from 31 to 31.7°S where the shelf is the

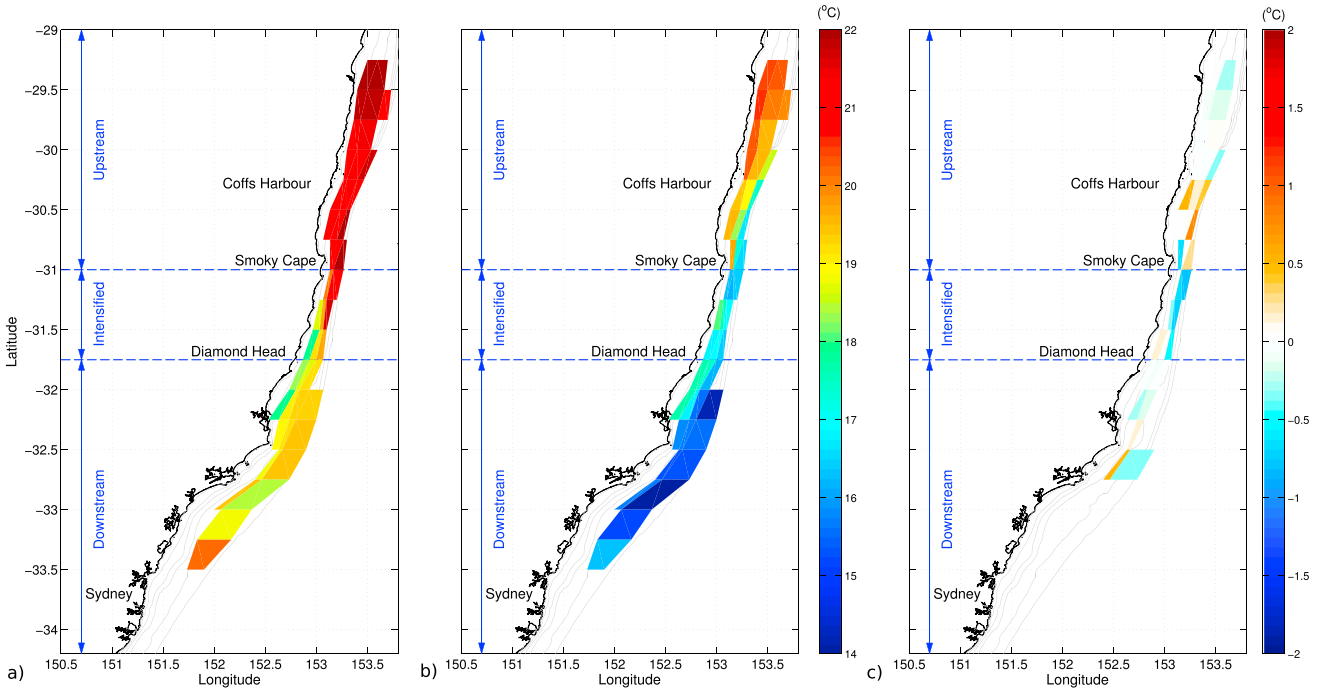


**Figure 2.** Binned mean temperature from glider profiles in (a) the top 20 m and (b) the bottom 20 m. (c) Difference of standard deviations between the surface and the bottom temperature (only for bins with more than four gliders). The coastline and isobaths (20, 50, 80, 110, 140, and 200 m) are also indicated (black and grey lines, respectively). The cross-shelf discretization corresponds to different depth ranges (20–50 m, 50–80 m, 80–110 m, 110–140 m, and 140–200 m).

narrowest, confirming the modeling studies of *Oke and Middleton* [2000] and *Roughan et al.* [2003]. The mean depth-averaged velocities (from an average of 4 to 10 gliders) are −0.21 to −0.53 m $s^{-1}$ over the shelf (isobath >50 m), and the ellipses show little variability in the across-shelf direction. We therefore refer to this region (31–31.7°S) as the intensified EAC zone, in contrast to upstream (north of 31°S) and downstream (south of 31.7°S). In the upstream and intensified zones the ellipses tend to be elongated in the along-shelf direction. This is in agreement with the variability observed from depth-averaged velocities measured by a bottom-mounted acoustic Doppler current profiler (8 m bins) at the mooring locations (Coffs Harbour, 30°S; Figure 1b). The mean depth-averaged current vectors as measured by the moorings (2010–2013) agree in direction but are greater in magnitude than those measured by the glider. Downstream, the current variance ellipses show enhanced variability, corresponding to the widening of the continental shelf, between 32 and 33°S and a weaker average current.

### 3.2. Influence on Hydrography

This climatology of temperature and salinity reveals the three-dimensional pattern of slope water uplift and the corresponding water masses associated with the separation of the EAC. The surface temperature pattern clearly shows the influence of the warm EAC adjacent to the coast in the upstream and intensified zones, where temperature ranges 20–22°C (Figure 2a). Upstream, cross-shelf temperature gradients are weak and the bottom waters are also relatively warm ranging 18.5–20.5°C, inshore of the 80 m isobath (Figure 2b), consistent with the prevailing influence of the EAC encroachment. The mean water mass characteristics for each glider and bin are presented in *T-S* space (Figure 3) where the mean surface and bottom temperature and salinity are associated with the corresponding velocity. On the *T-S* diagram, the prevalence of the EAC results in closely grouped symbols for each of the different glider deployments (Figure 3a) and bins across the shelf.

In the intensified zone, the maximum southward velocity corresponds to a higher cross-shelf surface temperature gradient (up to 2°C between the three first bins within less than 15 km; Figure 2a) and colder bottom temperatures (16–18°C; Figure 2b). The water mass characteristics show greater spread (Figure 3b), with the appearance of a bottom water mass with density greater than 26 kg $m^{-3}$ ($T < 16$°C, $S < 35.4$), reaching the 50–80 m isobaths (Figure 3b). This water is assumed to originate from below the EAC salinity

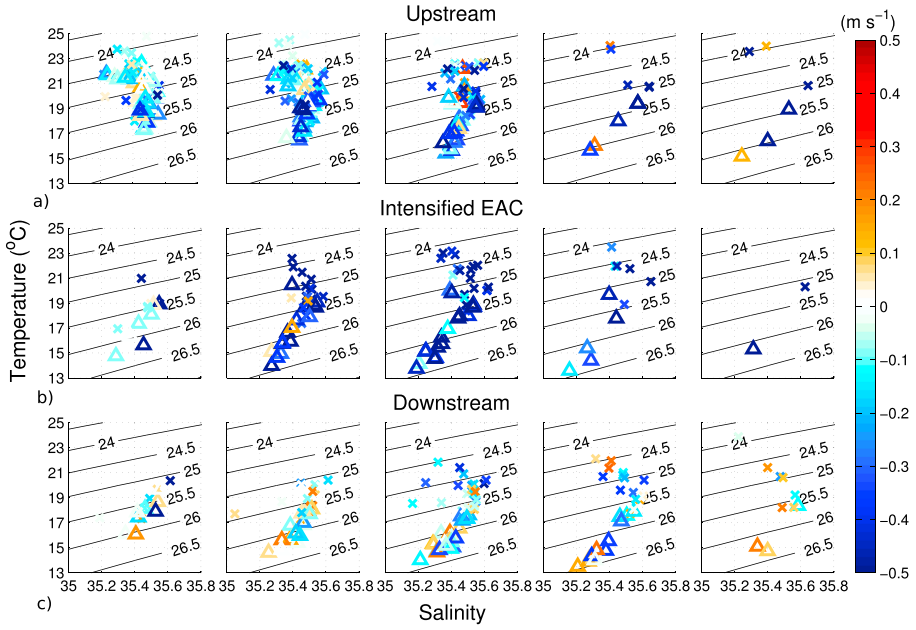


**Figure 3.** Averaged temperature-salinity plots for each glider and cross-shelf bin (columns: 20–50 m, 50–80 m, 80–110 m, 110–140 m, and 140–200 m) and different latitudinal bins (rows) representing the three zones, (a) upstream, (b) intensified EAC, and (c) downstream. Colors represent the depth-averaged velocity, and symbols represent the depth of the averaged observations from the top 20 m (cross) and the bottom 20 m (triangle). Density contours are shown as black solid lines.

maximum, being uplifted along the slope in response to the bottom stress driven by the intense EAC shelf encroachment, in agreement with results from *Schaeffer et al.* [2013, 2014a].

Downstream, where velocities are weaker and more variable (32°S–33.5°S), the mean bottom temperature is generally uniform over the shelf ranging 14–16°C (except for the inshore bins at 32°S). Salinity in this cold bottom water is consistent across the shelf, indicative of uplift (Figure 3c). Temperature variability is comparable in the bottom and surface layers, in contrast to the higher (mostly lower) bottom variability in the intensified (upstream) zone (Figure 2c). This suggests more intermittent uplift events in the intensified EAC zone and a more persistent pattern of bottom water uplift downstream, characteristic of the EAC separation. This is in agreement with modeling results from *Roughan et al.* [2003] showing a positive surface divergence maximum across the continental shelf south of 32°S.

### 3.3. Depth-Averaged Momentum Balances

This unique data set gives new insight into the depth-averaged momentum balances along the shelf spanning the EAC separation point. Here, we do not intend to resolve the temporal variability of the dynamical balance as we do not consider a continuous time series. However, we are able to estimate the relative dynamical balances in each of the three zones.

The depth-averaged cross-shelf and along-shelf momentum equations are as follows:

$$U_t - fV + UU_x + VU_y = -P_x/\rho_0 + (\tau^{sx} - \tau^{bx})/(\rho_0 H) \quad (1)$$

and

$$V_t + fU + UV_x + VV_y = -P_y/\rho_0 + (\tau^{sy} - \tau^{by})/(\rho_0 H) \quad (2)$$

where $(U, V)$ are the depth-averaged velocities in an eastward and northward $(x, y)$ coordinate system, $P$ is the depth-averaged pressure, $f$ is the Coriolis parameter, $\rho_0$ the reference water density taken as $\rho_0 = 1025\ \mathrm{kg\,m^{-3}}$, $\tau^{sx}$ and $\tau^{bx}$ ($\tau^{sy}$ and $\tau^{by}$) are the surface and bottom stress components along the $x$ ($y$) axis, respectively, and $H$ is the water depth. Subscripts indicate differentiation. The Coriolis ($-fV$ and $fU$) and advection ($UU_x$, $VU_y$ and $UV_x$, $VV_y$) terms are computed from the binned-averaged glider-derived velocities. Due to missing high-resolution information on the free surface elevation or bottom pressure values, only

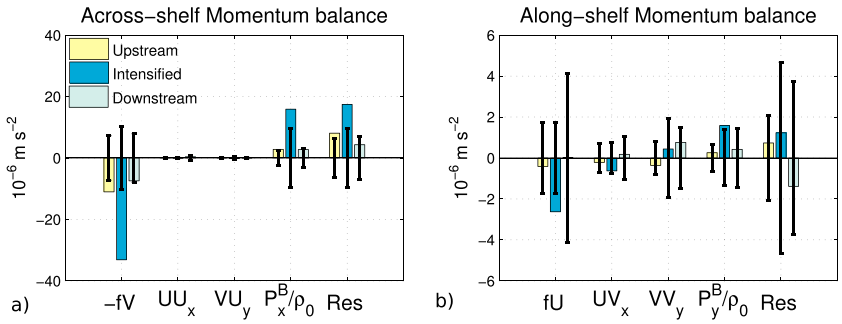


**Figure 4.** Mean (thick bars) and standard deviation (thin black bars) of the terms in (a) the depth-averaged across-shelf momentum equation (equation (1)) and (b) the depth-averaged along-shelf momentum equation (equation (2)) for the three different zones: upstream (<31°S, yellow), intensified EAC (31°S–31.7°S, blue), and downstream (>31.7°S, grey). Note that standard deviations show an estimate of the variance, not the error bar.

the baroclinic component [*Brown et al.*, 1985] of the pressure gradient terms ($P_x/\rho_0$ and $P_y/\rho_0$) is estimated as follows:

$$P^B_x/\rho_0 = g/(\rho_0 H)\int_{-H}^{0}\int_{z}^{0}\rho'_x dz'dz, \qquad P^B_y/\rho_0 = g/(\rho_0 H)\int_{-H}^{0}\int_{z}^{0}\rho'_y dz'dz$$

where $\rho(x,y,z)' = \rho(x,y,z) - \rho_0$ is the density anomaly.

As the local acceleration, stress, and barotropic pressure gradient terms could not be calculated directly from the glider data set, they are interpreted as part of the residual defined as minus the sum of the estimated terms, which also includes instrument and calculation errors.

This results in a binned map for each of the terms in the momentum balances from each glider mission (as in Figure 2). Due to the small number of gliders passing through each bin (0–11), we consider averages within the three zones. We focus on the magnitude of the standard deviations to determine the relative importance of each term (Figure 4) as in *Lentz et al.* [2014], while the mean values are included to demonstrate the sign of the different terms. This can be interpreted as a mean temporal representation of the three regimes: upstream, intensified EAC, and downstream.

In the across-shelf momentum balance, the results show a dominant geostrophic balance between the Coriolis and the sum of the residual and baroclinic pressure gradient terms, considering that the residual is mostly representative of the barotropic pressure gradient. In the upstream zone, standard deviations of $15\times10^{-6}$, $13\times10^{-6}$, and $5\times10^{-6}$ m s$^{-2}$ are calculated for Coriolis, residual, and baroclinic pressure gradient terms, respectively. This is in agreement with the findings of *Schaeffer et al.* [2013, 2014a], who used 3 years of moored observations at 30°S and found standard deviations of $16\times10^{-6}$, $14\times10^{-6}$, and $6\times10^{-6}$ m s$^{-2}$ for Coriolis, barotropic, and baroclinic pressure gradient terms, respectively. Both the advection terms are orders of magnitude smaller at this scale; we find a mean standard deviation of $UU_x$ of $0.5\times10^{-6}$ m s$^{-2}$ in the upstream zone (*Schaeffer et al.* [2013, 2014a] found $0.2\times10^{-6}$ m s$^{-2}$). The EAC intensified zone is characterized by the most important baroclinic pressure gradient which is predominantly positive (warm EAC offshore) and a strong negative Coriolis term indicating little along-shelf current reversal.

The standard deviations for the along-shelf momentum balance show that all terms make a substantial contribution with similar orders of magnitude. The mean Coriolis acceleration usually opposes the residual, while the importance of advection shows a strong nonlinearity. These are the first observations to confirm the findings of modeling results from *Oke and Middleton* [2000] and *Roughan et al.* [2003]. The importance and nature of advection varies along the shelf, being a maximum and along-shelf in the intensified EAC zone. In this region, the standard deviation for $VV_y$ is greater than the standard deviation for the Coriolis term, indicating intense nonlinear effects interfering with the geostrophic balance. The positive sign of $VV_y$ suggests a predominant advective deceleration of the southward flow in a Lagrangian sense (contrary to upstream), and the negative Coriolis term indicates a consistent offshore component. The positive mean of the baroclinic pressure gradient is related to the along-shelf density gradient enhanced just before the EAC

separation. Downstream, the dynamical balance reverses, confirming the modeling results of *Roughan et al.* [2003]. Coriolis and residual terms are the most important suggesting a more geostrophic adjustment. The high standard deviations compared to the magnitude of the means highlight the strong variability in the cross-shelf flow, in agreement with the topography and curved coastline orientation.

## 4. Discussion

While the dynamic nature of the region prohibits the occupation of endurance glider lines extending from the coast into the deep ocean as is the norm in other regions, we have presented a successful methodology inshore of a dynamic western boundary current, in a region of very narrow shelf topography. The compilation of the data from 23 glider deployments along the continental shelf enables new insights into the hydrography and dynamics in the EAC separation zone. This is a vast improvement upon the existing regional in situ climatology Commonwealth Scientific and Industrial Research Organisation Atlas of Regional Seas, [*Ridgway et al.*, 2002], which is based on fewer observations and characterized by a coarse horizontal resolution (0.5°) that does not adequately resolve the complex topographic and cross-shelf hydrographic structure. The main advantage of the ocean gliders and the deployment strategy presented here is the massive number of measurements (>30,000) and the high cross-shelf and vertical resolution.

We present the first high-resolution shelf mapping of the subsurface water mass characteristics of the EAC and its separation. The encroachment of the EAC dominates the depth-averaged circulation over the continental shelf upstream of 31.7°S and is a maximum between 31 and 31.7°S, where the shelf is the narrowest. This is where dense water $>$ 26 kg $m^{-3}$ appears in the bottom layer with a specific fresher and colder signature, suggesting slope water uplift in response to high bottom stress. Downstream, the current variability is higher and cold bottom temperatures with lower variability can be attributed to current-separation uplift events. Both these current-driven mechanisms have great implications for biology, driving nutrient input, Chlorophyll-a blooms [*Roughan and Middleton*, 2002], and changes in the phytoplankton community [*Armbrecht et al.*, 2014a, 2014b].

The EAC separation point has been shown to exhibit high temporal variability, oscillating between 28 and 37°S in the last 30 years [*Cetina-Heredia et al.*, 2014], having separated between 30 and 31.7°S 50% of the time since 1983. Smoky Cape (31°S, northern end of our intensified zone) was previously referred to as the EAC separation point by *Roughan et al.* [2003]. This is relevant in a dynamical sense, as the glider data confirm an advective deceleration and an offshore component of the flow between 31 and 31.7°S. However, both the shelf velocities and hydrography highlight the dominant influence of the southward flowing EAC in this region. Our results show a predominant separation from the continental shelf around 31.7°S in recent years.

The analysis of the glider bio-optical parameters will enable more insights into the biological response, while the ongoing glider deployments will enable further investigation into the robustness of the spatial patterns in the dynamical balances, as well as valuable data input for an updated high-resolution climatology, reanalysis products, and data assimilation modeling.

**Acknowledgments**

The operation and maintenance of the ocean glider fleet is managed by the Australian National Facility for Ocean Gliders (ANFOG) in the framework of the Australian Integrated Marine Observing System (IMOS). We appreciate the efforts of the IMOS glider teams in NSW and WA. We thank D. White for contribution to the development of the climatology. IMOS is an initiative of the Australian federal government funded under the National Collaborative Infrastructure Scheme and the Super Science Initiative. All data sets are available at http://www.imos.org.au. We thank two anonymous reviewers for their comments which have improved the quality of the manuscript.

The Editor thanks two anonymous reviewers for their assistance in evaluating this paper.

## References

Arbic, B. K., A. J. Wallcraft, and E. J. Metzger (2010), Concurrent simulation of the eddying general circulation and tides in a global ocean model, *Ocean Modell.*, *32*(3-4), 175–187, doi:10.1016/j.ocemod.2010.01.007.

Armbrecht, L. H., A. Schaeffer, M. Roughan, and L. K. Armand (2014a), Interactions between seasonality and oceanic forcing drive the phytoplankton variability in the tropical-temperate transition zone (~30°S) of Eastern Australia, *J. Mar. Syst.*, *144*, 92–106, doi:10.1016/j.jmarsys.2014.11.008.

Armbrecht, L. H., M. Roughan, V. Rossi, A. Schaeffer, P. L. Davies, A. M. Waite, and L. K. Armand (2014b), Phytoplankton composition under contrasting oceanographic conditions: Upwelling and downwelling (Eastern Australia), *Cont. Shelf Res.*, *75*, 54–67, doi:10.1016/j.csr.2013.11.024.

Baird, M. E., I. M. Suthers, D. A. Griffin, B. Hollings, C. Pattiaratchi, J. D. Everett, M. Roughan, K. Oubelkheir, and M. Doblin (2011), The effect of surface flooding on the physical-biogeochemical dynamics of a warm-core eddy off southeast Australia, *Deep Sea Res., Part II*, *58*(5), 592–605, doi:10.1016/j.dsr2.2010.10.002.

Brown, W. S., N. R. Pettigrew, and J. D. Irish (1985), The Nantucket shoals flux experiment (NSFE79). Part II: The structure and variability of across-shelf pressure gradients, *J. Phys. Oceanogr.*, *15*, 749–771.

Cetina-Heredia, P., M. Roughan, E. van Sebille, and M. A. Coleman (2014), Long-term trends in the east australian current separation latitude and eddy driven transport, *J. Geophys. Res. Oceans*, *119*, 4351–4366, doi:10.1002/2014JC010071.

Deng, X., D. Griffin, K. Ridgway, J. Featherstone, N. White, and M. Cahill (2010), Satellite altimetry for geodetic, oceanographic and climate studies in the Australian region, in *Coastal Altimetry*, edited by S. Vignudelli, pp. 473–508, Springer, Berlin.

Everett, J. D., M. E. Baird, M. Roughan, I. M. Suthers, and M. A. Doblin (2014), Relative impact of seasonal and oceanographic drivers on surface chlorophyll a along a western boundary current, *Prog. Oceanogr.*, *120*, 340–351, doi:10.1016/j.pocean.2013.10.016.

Lentz, S. J., B. Butman, and C. Harris (2014), The vertical structure of the circulation and dynamics in Hudson Shelf Valley, *J. Geophys. Res. Oceans*, *119*, 3694–3713, doi:10.1002/2014JC009883.

Mata, M., M. Tomczak, S. Wijffels, and J. Church (2000), East Australian Current volume transports at 30S: Estimates from the World Ocean Circulation Experiment hydrographic sections PR11/P6 and the PCM3 current meter array, *J. Geophys. Res.*, *105*(C12), 28,509–28,526.

Mata, M., S. Wijffels, J. Church, and M. Tomczak (2006), Statistical description of the East Australian Current low-frequency variability from the WOCE PCM3 array, *Mar. Freshwater Res.*, *57*(3), 273–290.

Merckelbach, L., R. D. Briggs, D. Smeed, and G. Griffiths (2008), Current measurements from autonomous underwater gliders, in *IEEE/OES 9th Working Conference Current Measurement Technology (CMTC)*, pp. 61–67, IEEE, Charlston, S. C., doi:10.1109/CCM.2008.4480845.

Oke, P. R., and J. H. Middleton (2000), Topographically induced upwelling off Eastern Australia, *J. Phys. Oceanogr.*, *30*(3), 512–531.

Oke, P. R., and J. H. Middleton (2001), Nutrient enrichment off Port Stephens: The role of the East Australian Current, *Cont. Shelf Res.*, *21*(6–7), 587–606, doi:10.1016/S0278-4343(00)00127-8.

Oke, P. R., and P. Sakov (2012), Assessing the footprint of a regional ocean observing system, *J. Mar. Syst.*, *105-108*, 30–51, doi:10.1016/j.jmarsys.2012.05.009.

Oke, P. R., M. England, and J. Middleton (2003), On the dynamics of an observed thermal front off Central Eastern Australia, *J. Geophys. Res.*, *108*(C4), 3106, doi:10.1029/2002JC001370.

Oliver, E., and N. Holbrook (2014), Extending our understanding of South Pacific gyre "spin-up": Modeling the East Australian Current in a future climate, *J. Geophys. Res. Oceans*, *1-18*, 2788–2805, doi:10.1002/2013JC009591.

Ridgway, K. R., J. R. Dunn, and J. L. Wilkin (2002), Ocean interpolation by four-dimensional weighted least squares—Application to the waters around Australasia, *J. Atmos. Oceanic Technol.*, *19*, 1357–1375.

Ridgway, K. R., R. Coleman, R. Bailey, and P. Sutton (2008), Decadal variability of East Australian Current transport inferred from repeated high-density XBT transects, a CTD survey and satellite altimetry, *J. Geophys. Res.*, *113*, C08039, doi:10.1029/2007JC004664.

Rossi, V., A. Schaeffer, J. Wood, G. Galibert, B. Morris, J. Sudre, M. Roughan, and A. M. Waite (2014), Seasonality of sporadic physical processes driving temperature and nutrient high-frequency variability in the coastal ocean off southeast Australia, *J. Geophys. Res. Oceans*, *119*, 445–460, doi:10.1002/2013JC009284.

Roughan, M., and J. H. Middleton (2002), A comparison of observed upwelling mechanisms off the East Coast of Australia, *Cont. Shelf Res.*, *22*(17), 2551–2572, doi:10.1016/S0278-4343(02)00101-2.

Roughan, M., and J. H. Middleton (2004), On the East Australian Current: Variability, encroachment, and upwelling, *J. Geophys. Res.*, *109*, C07003, doi:10.1029/2003JC001833.

Roughan, M., P. R. Oke, and J. H. Middleton (2003), A modelling study of the climatological current field and the trajectories of upwelled particles in the East Australian Current, *J. Phys. Oceanogr.*, *33*(12), 2551–2564.

Rudnick, D. L., S. Jan, L. Centurioni, C. Lee, R.-C. Lien, J. Wang, D.-K. Lee, R.-S. Tseng, Y. Kim, and C.-S. Chern (2011), Seasonal and mesoscale variability of the Kuroshio near its origin, *Oceanography*, *24*(4), 52–63, doi:10.5670/oceanog.2011.94.

Schaeffer, A., M. Roughan, and B. Morris (2013), Cross-shelf dynamics in a Western Boundary Current. Implications for upwelling, *J. Phys. Oceanogr.*, *43*, 1042–1059, doi:10.1175/JPO-D-12-0177.1.

Schaeffer, A., M. Roughan, and B. D. Morris (2014a), CORRIGENDUM, *J. Phys. Oceanogr.*, *44*, 2812–2813, doi:10.1175/JPO-D-14-0091.1.

Schaeffer, A., M. Roughan, and J. E. Wood (2014b), Observed bottom boundary layer transport and uplift on the continental shelf adjacent to a western boundary current, *J. Geophys. Res. Oceans*, *119*, 4922–4939, doi:10.1002/2013JC009735.

Suthers, I. M., et al. (2011), The strengthening East Australian Current, its eddies and biological effects—An introduction and overview, *Deep Sea Res., Part II*, *58*(5), 538–546, doi:10.1016/j.dsr2.2010.09.029.

Wong, A., R. Keeley, T. Carval, and Argo Data Management Team (2014), *Argo Quality Control Manual*, Ifremer, France, doi:10.13155/33951.

Wood, J. E., M. Roughan, and P. M. Tate (2013), Annual cycling in wind, temperature and along shore currents on the Sydney shelf, in *Proceedings of Coasts and Ports: 21st Australasian Coastal and Ocean Engineering Conference and the 14th Australasian Port and Harbour Conference*, pp. 866–871, Julie Wood, Sydney, Australia.